The Role of Perceptual Texture Dissimilarity in Automating Seismic Data Interpretation

Tamir Hegazy, Zhen Wang and Ghassan AlRegib
Center for Energy and Geo Processing (CeGP) at Georgia Tech and KFUPM
School of Electrical and Computer Engineering, Georgia Institute of Technology
Atlanta, GA , USA
{th164, zwang313, alregib}@gatech.edu

***Abstract*—Automating the interpretation of post-migrated seismic data would considerably reduce the time and cost of the interpretation process. In this paper, we study the role of texture perception in automating the delineation of an important sub-surface structure: salt dome. First, we propose a new seismic attribute, the gradient of texture, based on which we develop a framework for detecting and delineating salt domes. Since the new attribute can be defined based on a variety of dissimilarity measures, we define a perceptual dissimilarity measure and compare its performance against several other perceptual and non-perceptual texture dissimilarity measures in delineating salt domes in a real seismic data set. Our experimental evaluation reveals that results based perceptual measures are more consistent with human-interpreted results. Therefore, an important contribution of this paper is confirming that the human interpretation process does not only rely on geological and geophysical knowledge, but it also relies on the visual perception of 2D seismic data. Further, the proposed perceptual dissimilarity measure yields the best result and computational efficiency among all studied measures.**

***Index Terms*—texture perception, gradient of texture, salt dome interpretation**

I. Introduction and Related Work

Salt domes are important geological structures in the oil and gas exploration industry because their impermeability leads to the formation of oil and gas reservoirs. To locate such reservoirs, a team of experienced interpreters visually examine seismic data for a long time (several months). Automating parts of the interpretation process could considerably reduce the time and hence the cost of the interpretation process. As a result, researchers have contributed several methods to help automate the detection and delineation of salt domes. In this paper, we focus on evaluating the role of texture perception in automating the interpretation process of salt domes.

Existing salt dome detection methods include normalized cut image segmentation (NCIS) [1]. Lomask *et al.* [2] proposed NCIS to globally optimize the delineation of salt dome boundaries. As an extension of this method, [3] utilized bound constraints to remove boundary artifacts. Similarly, Halpert *et al.* [4] introduced the modified NCIS by combining multiple seismic attributes with adaptive weights. The high computational cost limits their future application on high-resolution data. To improve the efficiency of global segmentation, Halpert *et al.* [5] proposed to detect the boundaries of salt domes using a pairwise region comparison based on the minimum spanning tree [6], which reduces the algorithm complexity.

In addition to the segmentation-based methods, edge detection has also been explored. Zhou *et al.* [7] and Aqrawi *et al.* [8] applied dip-guided 2D and 3D Sobel filters to detect salt dome boundaries in time slices, respectively. Recently, Berthelot *et al.* [9] have proposed to delineate salt domes through a combination of multiple attributes (i.e., texture, frequency, and dip) in a supervised Bayesian classification model. To characterize the homogeneous texture of salt bodies, the method in [10] shows that a few seismic attributes could be sufficient for salt dome detection and boundary delineation.

In this paper, we define a texture-based attribute, the gradient of texture (GoT), based on texture dissimilarity between neighboring texture windows. Then, we develop a processing framework for detection and delineation of salt dome boundaries based on the GoT attribute. The GoT attribute and the framework are independent of the choice of the defined dissimilarity measure. We propose a computationally efficient perceptual dissimilarity measure and compare it against other perceptual and non-perceptual dissimilarity measures. The comparison shows that using perceptual dissimilarity measures yields results that are more consistent with the human interpreted results. Further, the proposed dissimilarity measure proves to deliver results that are the most consistent with human interpretation, while being the most computationally efficient among all considered dissimilarity measures.

The rest of the paper is organized as follows. First, we introduce the GoT attribute, the processing framework, and the various dissimilarity measures in Sec. II. Then, we present and discuss the experimental results in Sec. III. Finally, we conclude the paper in Sec. IV.

II. Proposed Salt Dome Detection Method

As opposed to the top boundary of a salt dome, which appears in migrated seismic surveys as areas with high contrast and strong edges due to the cap rock, side boundaries usually lack such edges and are more difficult to detect (Fig. 1). However, seismic interpretation experts would still be able to visually delineate such boundary using the change of texture between salt and non-salt regions. As a matter of fact, non-experts can still perceptually differentiate between the two regions and possibly draw a boundary line. Therefore, we believe that an automated method should take human visual perception into account.

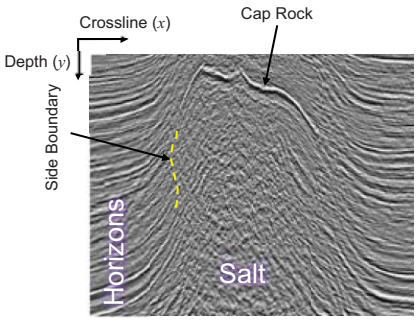

Fig. 1: Salt dome boundaries lacking strong edges.

Our proposed processing framework consists of the following steps:

1) Computing the GoT attribute for a given seismic section.
2) Enhancing contrast and smoothing the attribute map.
3) Thresholding the enhanced attribute map.
4) Growing salt region from an initialization point.
5) Performing binary morphology to clean up and adjust the detected salt region.

In the following subsections, we explain each step in detail.

A. Gradient of Texture

We define the GoT at a given point as the dissimilarity between two square neighborhood windows that share a side centered around the given point. The shared side is perpendicular to the direction of interest [11][12]. Fig. 2 illustrates an example with two texture regions separated by a purely vertical boundary. For a given row, if we slide the center point (and hence the two neighborhood windows in the figure) along the horizontal direction, we expect the GoT profile to follow the curve shown at the bottom of the figure. For other rows, we expect similar curves because the boundary is purely vertical in this example. Theoretically, the highest dissimilarity, and hence the highest GoT value, is obtained when the center point falls exactly on the texture boundary because the left neighborhood window $\mathbf{W}_{x-}$ will have completely different texture content from that of the right neighborhood window $\mathbf{W}_{x+}$. When we move the center point away from the texture boundary to the position shown in Fig. 2, the content of W_{x+} is purely from the right-hand side texture region, while $\mathbf{W}_{x-}$ contains both textures. The partially shared content will cause the dissimilarity value, and hence the GoT value, to drop. If we keep moving the center point along with the neighborhood windows away from the boundary, we reach a point where the contents of both W_{x-} and $\mathbf{W}_{x+}$ are from the same texture region; i.e., the texture contents will be exactly similar. This exact similarity means zero dissimilarity, and hence, zero GoT.

For the texture boundary in Fig. 2, computing the GoT in the horizontal direction is sufficient because the texture boundary is purely vertical. For the general case, we compute the GoT as a vector with components in both the horizontal and vertical directions. Fig. 3 shows how the gradient of texture is computed for the general case. The neighborhood windows marked with solid lines are used to compute the horizontal GoT component, while those marked with dashed lines are

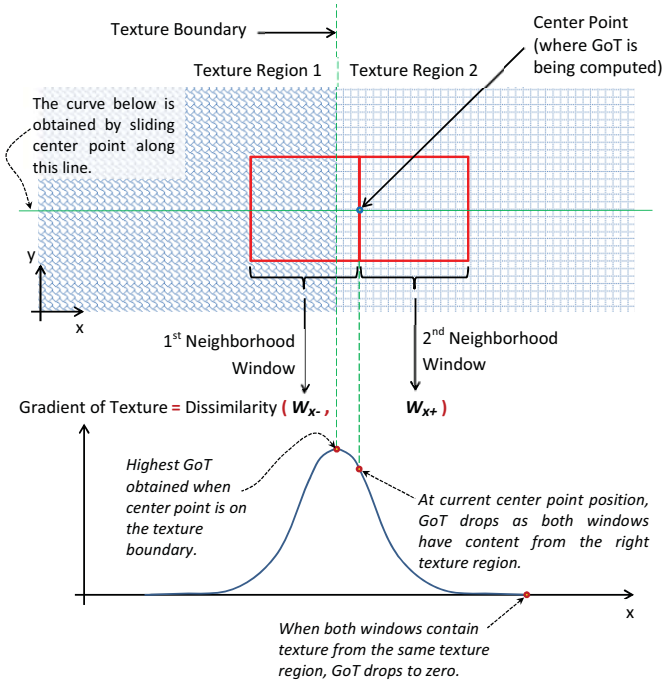

Fig. 2: GoT at a given point represents the dissimilarity between two square neighborhood windows.

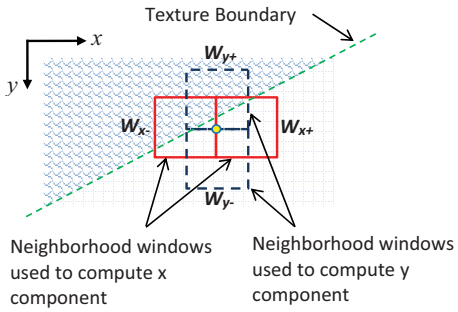

Fig. 3: Neighborhood windows used to compute GoT int he horizontal and vertical directions.

used to compute the vertical component. With the large scale variations in texture content, the neighborhood window size used to compute GoT needs to be carefully chosen. To improve robustness, we use different window sizes (5 in our case) and we choose the weighted average of the quantities as the attribute value. The neighborhood window sizes range from 3×3 to 11×11. Fig. 4 shows neighborhood windows of minimum and maximum sizes around a labeled salt dome boundary. Note that different window sizes enable capturing texture dissimilarity across different scales. The multi-scale GoT is mathematically expressed as follows:

$$\mathbf{G}_{\mathbf{x}}[i,j] = \sum_{n=1}^{N} w_n . d\left(\mathbf{W}_{n,x-}^{i,j}, \mathbf{W}_{n,x+}^{i,j}\right), \tag{1}$$

$$\mathbf{G}_{\mathbf{y}}[i,j] = \sum_{n=1}^{N} w_n . d\left(\mathbf{W}_{n,y-}^{i,j}, \mathbf{W}_{n,y+}^{i,j}\right), \tag{2}$$

$$\mathbf{G}[i,j] = \left(\mathbf{G}_{\mathbf{x}}{}^2[i,j] + \mathbf{G}_{\mathbf{y}}{}^2[i,j]\right)^{\frac{1}{2}}, \tag{3}$$

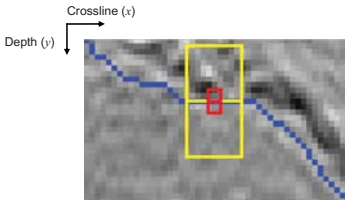

Fig. 4: Neighborhood windows of minimum size (3×3) and maximum size (11×11) shown around a salt dome boundary.

where $\mathbf{G_x}[i,j]$ and $\mathbf{G_y}[i,j]$ denote the GoT values at point $[i,j]$ along the horizontal and vertical directions respectively, $\mathbf{G}[i,j]$ represents the GoT value combining the horizontal and vertical components, function $d(\cdot)$ defines a dissimilarity measure, and the four $\mathbf{W}^{i,j}$ expressions with four different subscripts refer to the four neighborhood windows shown in Fig. 3. In our case, $N=5$. Also, for a given n, the neighborhood window size is $(2n+1)\times(2n+1)$, and $\mathbf{W}^{i,j}_{n,x-}$, $\mathbf{W}^{i,j}_{n,x+}$, $\mathbf{W}^{i,j}_{n,y-}$, $\mathbf{W}^{i,j}_{n,y+}$ respectively denote the neighborhood windows of size $(2n+1)\times(2n+1)$ that are to the left, right, bottom and top of the point $[i,j]$ where the attribute is being computed. Finally, w_n denotes the weight of the GoT value computed at the window whose size is $(2n+1)\times(2n+1)$.

B. Dissimilarity Measures

To measure the dissimilarity between neighboring windows, we evaluate the following five dissimilarity measures. The last two measures are strongly correlated with human perception [10].

1) Measure Based on Intensity and Gradient Statistics: For the two neighborhood windows $\mathbf{W}_-$ and $\mathbf{W}_+$, we compute feature vectors $\mathbf{F}_-$ and $\mathbf{F}_+$, respectively. The vector components are based on:

- Three intensity-based features: mean, standard deviation and skewness.
- Three gradient-based features: mean, standard deviation, and entropy.

Then, we define the dissimilarity measure as the norm of the difference between the vectors:

$$d(\mathbf{W}_-,\mathbf{W}_+)=\|\mathbf{F}_- - \mathbf{F}_+\|. \tag{4}$$

2) Measure Based on Singular Values: For the neighborhood window $\mathbf{W}_-$, we compute the singular value decomposition $\mathbf{W}_- = \mathbf{U}\mathbf{\Sigma}\mathbf{V}^T$, and compose feature vector $\mathbf{F}_-$ similar to the method proposed in [13]. $\mathbf{F}_-$ contains the sorted diagonal elements of the diagonal matrix $\mathbf{\Sigma}_-$. Similarly, we compute the feature vector $\mathbf{F}_+$ for the neighborhood window $\mathbf{W}_+$. Then, we define the dissimilarity measure as shown in Eq. (4).

3) Measure Based on Fourier Coefficients: For each of the two neighborhood windows, we compute the 2D DFT. Then, we compute the dissimilarity measure as the mean of absolute difference between the magnitude spectra of the two windows:

$$d(\mathbf{W}_-,\mathbf{W}_+)=E\left\{\left|\left|\mathscr{F}\left\{\mathbf{W}_-\right\}\right|-\left|\mathscr{F}\left\{\mathbf{W}_+\right\}\right|\right|\right\}, \tag{5}$$

where $\mathscr{F}\{\cdot\}$ denotes the 2D DFT, and $E\{\cdot\}$ denotes the expectation operator.

4) Perceptual Measure Based on Error Spectrum Chaos: This measure is introduced in [10], which was shown to be consistent with human perception while being computationally efficient. The dissimilarity measure characterizes the amount of variation, or chaos, in the magnitude and the phase spectra of the absolute error between the two windows. Since the proposed dissimilarity measure is highly consistent with human perception [10], we believe it partially imitates how the human interpreter delineates the salt boundaries according to the texture variations inside and outside the salt region. The measure is computed as follows:

$$d(\mathbf{W}_-,\mathbf{W}_+)=M+\alpha P, \tag{6}$$

$$M=E\left\{\left|\mathscr{F}\left\{\left|\mathscr{F}\left\{\nabla\left\{\left|\mathbf{W}_- - \mathbf{W}_+\right|\right\}\right\}\right|\right\}\right|\right\}, \tag{7}$$

$$P=E\left\{\left|\mathscr{F}\left\{\angle\mathscr{F}\left\{\left|\mathbf{W}_- - \mathbf{W}_+\right|\right\}\right\}\right|\right\}, \tag{8}$$

where $\mathscr{F}\{\cdot\}$ denotes the 2D DFT, E is the expectation operator, ∇ is the gradient operator, $\mathbf{W}_-$, $\mathbf{W}_+$ denote the two neighboring windows whose dissimilarity is to be evaluated, and α is a weight factor.

5) Proposed Perceptual Measure Based on Error Magnitude Spectrum Chaos: This measure is inspired by the previous measure in II-B4. We propose to takes into account the magnitude spectrum only ($\alpha=0$). The rationale behind dropping the phase is that the phase is responsible for shape. In the meantime, texture, especially in seismic data, is defined by statistical measures and is forgiving for exact accurate shapes. Consequently, dropping phase distortion makes the dissimilarity measure less sensitive to shape, while speeding up the GoT computation. Further, this measure drops the gradient operator used in the previous measure to further reduce the computation time without compromising the performance as we show later in Sec. III. Thus, the proposed measure is simply computed as follows:

$$d(\mathbf{W}_-,\mathbf{W}_+)=E\left\{\left|\mathscr{F}\left\{\left|\mathscr{F}\left\{\left|\mathbf{W}_- - \mathbf{W}_+\right|\right\}\right|\right\}\right|\right\}. \tag{9}$$

C. Initialization, Region Growing, and Thresholding

GoT detects several texture boundaries including ones outlining salt and others that are irrelevant to salt, e.g., from strong reflectors that are away from the salt dome. In order for the detection method to focus on the salt boundaries only, we identify an initialization point inside the salt dome and then use region growing until a predefined threshold for GoT magnitude is encountered. We assume interactive selection of initialization point, which is common in seismic interpretation industry. The time spent by human interpreter will be considerably reduced since the interpreter would have to quickly click on *any* arbitrary point within the salt region, as opposed to carefully traversing a long, tortuous salt dome boundary. The initialization point must fall inside the salt region, but is otherwise arbitrary. The proposed method is not sensitive to the initialization point selection as long as it falls inside the salt region.

Since the initialization point is inside the salt dome, i.e., inside a texture region, we expect the texture gradient around the initialization point to be very low (theoretically zero).

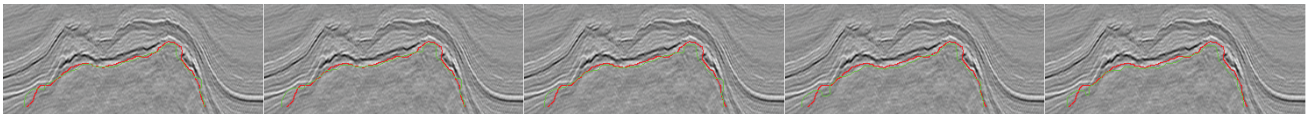

(a) Mag. spectrum Chaos SalSIM = 0.9471 (b) Spectrum chaos SalSIM = 0.9389 (c) Fourier coefficients SalSIM = 0.9405 (d) SVD SalSIM = 0.9293 (e) Basic statistics SalSIM = 0.9362

Fig. 5: Comparing delineation results (green) against ground truth (red) for section #404.

Thus, the initialization point can be grown since GoT in the neighboring region is less than a certain threshold value. The threshold value can be determined automatically or interactively with a human interpreter. We propose a hybrid approach where the value of the threshold is determined based on Otsu's method [14]. Then, we manually fine tune the threshold value. As we grow the region, we start meeting points that are close to the boundary of the dome where the GoT value is high. We stop growing along those points that reached the threshold of the GoT map.

III. Experimental Evaluation

A. Experimental Setup

In this paper, to investigate the performance of various dissimilarity measures in real seismic dataset, we focus on a local volume of the dataset acquired from the Netherlands offshore F3 block in the North Sea [15]. The tested volume contains discernible salt-dome structures and has an inline number ranging from #389 to #409, a crossline number ranging from #401 to #701, and a time direction ranging from 1,300ms to 1,848ms with a step of 4ms. To evaluate the performance of the proposed method, we employ a salt dome similarity (SalSIM) index [16] that measures the distances between semi-automatically labeled results and the ground truth provided by experienced interpreters. The SalSIM index is developed based on the Fréchet distance [17], which can more accurately measure the deviation between two curves than the Haudorff distance [18] by taking the continuity of curves into account.

B. Experimental Results

In terms of the SalSIM index, Table I shows the performance of the proposed method for 21 consecutive seismic sections under the five dissimilarity measures discussed in Sec. II-B. Overall, the dissimilarity measure based on the magnitude spectrum chaos yields the best mean SalSIM value of 0.9375 and the second best standard deviation of the SalSIM values. The second best dissimilarity measure is the one based on both magnitude and phase chaos, which yielded a mean SalSIM value of 0.9335. While including phase spectrum proved beneficial in natural image quality assessment applications [10], it makes the GoT attribute more sensitive to shape, which is undesirable for the application at hand. Seismic texture does not maintain regular patterns and is rather defined by statistical features as opposed to shape. It is noteworthy that perceptual dissimilarity measures lead to better performance when compared to non-perceptual ones. This confirms our intuition that seismic interpretation by human experts is not only based on geological/geophysical knowledge, but also on human perception, including texture dissimilarity perception. Table I also the GoT computation time per section using Matlab on 64-bit Windows 7 on Intel Core i5-3230M CPU @ 2.6 GHz. The magnitude spectrum chaos method is the fastest.

Fig. 5 shows the delineation results for seismic section #404 under the 5 dissimilarity measure considered in this paper. The corresponding SalSIM values are also given. The (green line) result in Fig. 5a, which is obtained by using the dissimilarity measure that is based on magnitude spectrum chaos, delivers the closest result to the ground truth (red).

TABLE I: SalSIM indices for various dissimilarity measures.

Seismic Sections	Mag. Spect. Chaos	Spectrum Chaos	Fourier Coeff.	SVD	Basic Statistics
#389	**0.9091**	0.9064	0.9050	0.8693	0.8440
#390	**0.9198**	0.9148	0.9186	0.8995	0.8406
#391	0.8930	0.8876	**0.9037**	0.8931	0.8585
#392	0.9312	**0.9354**	0.9345	0.9180	0.9221
#393	0.9331	**0.9345**	0.9283	0.8824	0.8546
#394	**0.9302**	0.9260	0.9267	0.9162	0.9283
#395	**0.9448**	0.9415	0.9337	0.9191	0.9213
#396	**0.9419**	0.9321	0.9283	0.9164	0.9228
#397	**0.9313**	0.9273	0.9230	0.9108	0.8586
#398	**0.9464**	0.9453	0.9369	0.9306	0.9282
#399	0.9435	**0.9447**	0.9402	0.9278	0.9432
#400	**0.9329**	0.9326	0.9303	0.9252	0.9230
#401	**0.9552**	0.9484	0.9507	0.9480	0.9471
#402	**0.9532**	0.9490	0.9501	0.9487	0.9488
#403	**0.9512**	0.9500	0.9506	0.9428	0.9377
#404	**0.9471**	0.9389	0.9405	0.9293	0.9362
#405	**0.9456**	0.9438	0.9391	0.9156	0.9055
#406	**0.9550**	0.9481	0.9461	0.9545	0.9487
#407	**0.9461**	0.9417	0.9434	0.9380	0.9394
#408	**0.9332**	0.9196	0.9298	0.9255	0.9188
#409	0.9430	0.9408	**0.9438**	0.9382	0.9287
Mean	**0.9375**	0.9337	0.9335	0.9214	0.9122
Standard. Dev.	0.0151	0.0155	**0.0129**	0.0213	0.0358
GoT Time per Section (s)	**14.5**	438.8	14.8	24.2	1359.2

IV. Conclusion

In this paper, we investigated the role of texture dissimilarity perception in the automatic interpretation of salt domes in seismic data. We used the proposed processing framework to evaluate the impact of 5 perceptual and non-perceptual dissimilarity measures. We conclude that perceptual measures deliver results that are more consistent with human interpretation.

V. Acknowledgements

This work is supported by the Center for Energy and Geo Processing (CeGP) at Georgia Tech and by King Fahd University of Petroleum and Minerals (KFUPM).

REFERENCES

[1] Jianbo Shi and Jitendra Malik, "Normalized cuts and image segmentation," *Pattern Analysis and Machine Intelligence, IEEE Transactions on*, vol. 22, no. 8, pp. 888–905, 2000.

[2] Jesse Lomask, Biondo Biondi, and Jeff Shragge, "Image segmentation for tracking salt boundaries," in *Expanded Abstracts of the SEG 74th Annual Meeting*, 2004, pp. 2443–2446.

[3] Jesse Lomask, Robert G. Clapp, and Biondo Biondi, "Application of image segmentation to tracking 3D salt boundaries," *Geophysics*, vol. 72, no. 4, pp. P47–P56, 2007.

[4] Adam D. Halpert, Robert G. Clapp, and Biondi, "Seismic image segmentation with multiple attributes," in *Expanded Abstracts of the SEG 79th Annual Meeting*. Society of Exploration Geophysicists, 2009, pp. 3700–3704.

[5] Adam D. Halpert, Robert G. Clapp, and Biondo Biondi, "Speeding up seismic image segmentation," in *Expanded Abstracts of the SEG 80th Annual Meeting*. Society of Exploration Geophysicists, 2010, pp. 1276–1280.

[6] Pedro F. Felzenszwalb and Daniel P. Huttenlocher, "Efficient graph-based image segmentation," *International Journal of Computer Vision*, vol. 59, no. 2, pp. 167–181, 2004.

[7] Jing Zhou, Yanqing Zhang, Zhigang Chen, and Li Jianhua, "Detecting boundary of salt dome in seismic data with edge detection technique," in *Expanded Abstracts of the SEG 80th Annual Meeting*. Society of Exploration Geophysicists, 2007, pp. 1392–1396.

[8] Ahmed Adnan Aqrawi, Trond Hellem Boe, and Sergio Barros, "Detecting salt domes using a dip guided 3D Sobel seismic attribute," in *Expanded Abstracts of the SEG 81st Annual Meeting*. Society of Exploration Geophysicists, 2011.

[9] Angélique Berthelot, Anne HS Solberg, and Leiv-J Gelius, "Texture attributes for detection of salt," *Journal of Applied Geophysics*, vol. 88, pp. 52–69, 2013.

[10] Tamir Hegazy and Ghassan AlRegib, "Texture attributes for detecting salt bodies in seismic data," in *Expanded Abstracts of the SEG 84th Annual Meeting*. Society of Exploration Geophysicists, 2014, pp. 1455–1459.

[11] Rafael Gonzalez and Richard Woods, *Digital Image Processing (3rd Edition)*, Prentice-Hall, Inc., Upper Saddle River, NJ, USA, 2006.

[12] Maria Petrou and Costas Petrou, *Image Processing: The Fundamentals*, John Wiley & Sons, 2010.

[13] L Tomczak and V Mosorov, "Singular value decomposition for texture defect detection in visual inspection systems," in *Proc. of the 2nd International Conference on Perspective Technologies and Methods in MEMS Design, 2006*, May 2006, pp. 131–133.

[14] Nobuyuki Otsu, "A threshold selection method from gray-level histograms," *IEEE Transactions on Systems, Man, and Cybernetics*, vol. 9, no. 1, pp. 62–66, 1979.

[15] Opendtect, "Netherland Offshore F3 Block Complete," http://www.opendtect.org/index.php/share-seismic-data/osr.html.

[16] Zhen Wang, Tamir Hegazy, Zhiling Long, and Ghassan AlRegib, "Noise-robust detection and tracking of salt domes in post-migrated volumes using texture, tensors, and subspace learning," .

[17] H. Alt and M. Godau, "Computing the Fréchet distance between two polygonal curves," *International Journal of Computational Geometry & Applications*, vol. 5, no. 01–02, pp. 75–91, 1995.

[18] D. P. Huttenlocher, G. A. Klanderman, and W. J. Rucklidge, "Comparing images using the Hausdorff distance," *Pattern Analysis and Machine Intelligence, IEEE Transactions on*, vol. 15, no. 9, pp. 850–863, 1993.